The reduction of biological production induced by mesoscale mixing: a modelling study in the Benguela upwelling.

Ismael Hernández-Carrasco[a,*], Vincent Rossi[b,c], Emilio Hernández-García[a], Veronique Garçon[b], Cristóbal López[a,*]

[a] *IFISC, Instituto de Física Interdisciplinar y Sistemas Complejos (CSIC-UIB), 07122 Palma de Mallorca, Spain*

[b] *Laboratoire d'Études en Géophysique et Océanographie Spatiale, CNRS, Observatoire Midi-Pyrénées, 14 avenue Edouard Belin, Toulouse, 31401 Cedex 9, France*

[c] *University of New South Wales, School of Maths and Statistics, Applied, Coastal Oceanography, Sydney 2052, AUSTRALIA*

Abstract

Recent studies, both based on remote sensed data and coupled models, showed a reduction of biological productivity due to vigorous horizontal mixing in upwelling systems. In order to better understand this phenomenon, we have considered a system of oceanic flow in the Benguela area coupled with a simple biogeochemical model of Nutrient-Phyto-Zooplankton (NPZ) type. For the flow three different surface velocity fields are considered: one derived from satellite altimetry data, and the other two from a regional numerical model at two different spatial resolutions. We computed horizontal particle dispersion in terms of Lyapunov Exponents, and analyzed their correlations with phytoplankton concentrations. Our modelling approach confirms that in the south Benguela, there is a reduction of biological activity when stirring is increased. Two-dimensional offshore advection seems to be the dominant process involved. In the northern area, other factors not taken into account in our simulation are influencing the ecosystem. We provide explanations for these results in the context of studies performed in other Eastern Boundary upwelling areas.

*Corresponding author. Tel.: +34 971 172668

Email addresses: ismael@ifisc.uib-csic.es (Ismael Hernández-Carrasco), clopez@ifisc.uib-csic.es (Cristóbal López)

1. Introduction

Marine ecosystems of the Eastern Boundary Upwelling zones are well known for their major contribution to the world ocean productivity. They are characterized by wind-driven upwelling along the coast of cold nutrient-rich waters that supports elevated plankton and pelagic fish production (Mackas et al., 2006). Variability is introduced by strong advection along the shore, physical forcings by local and large scales winds, and high sub- and mesoscale activities over the continental shelf and beyond, linking the coastal domain with the open ocean.

The Benguela Upwelling System (BUS) is one of the four major Eastern Boundary Systems (EBUS) of the world. The coastal area of the Benguela ecosystem extends from southern Angola (around 17°S) along the west coast of Namibia and South Africa (36°S). It is surrounded by two warm temperate boundary currents, the Angola Current in the north, and the Agulhas Current in the south. The BUS can itself be subdivided into two subdomains by the powerful Luderitz upwelling cell (Hutchings et al., 2009). Most of the biogeochemical activity occurs within the upwelling front and the coast, although it can be extended further offshore toward the open ocean by the numerous filamental structures developing offshore (Monteiro, 2009). In the BUS, as in the other major upwelling areas, a high mesoscale activity due to eddies and filaments is observed and impacts strongly on marine planktonic ecosystem over the shelf and beyond (Brink and Cowles, 1991; Martin, 2003; Sandulescu et al., 2008; Rossi et al., 2009).

The purpose of this study is to analyze the impact of the horizontal stirring on the phytoplankton dynamics in the BUS. Recently, Rossi et al. (2008, 2009), using satellite data of the ocean surface, suggested that mesoscale activity has a negative effect on chlorophyll standing stocks in the EBUS. This was obtained by correlating remote sensed chlorophyll data with a Lagrangian measurement of lateral stirring in the surface ocean (see Methods section below). This result was unexpected since mesoscale transport, particularly due to eddies, has been related to higher planktonic production and stocks in the open ocean

(McGillicuddy et al., 2007) as well as off a major EBUS (Correa-Ramirez et al., 2007). A more recent and thorough study performed by Gruber et al. (2011) in the California and the Canary current systems detailed the initial results from Rossi et al. (2008, 2009). Based on satellite derived estimates of net Primary Production, of upwelling strength and of Eddy Kinetic Energy (EKE) as a measure the intensity of mesoscale activity, they confirmed the suppressive effect of mesoscale structures on biological production in upwelling areas. The mechanism behind this observation was investigated using 3D eddy resolving coupled models. The eddies tend to export offshore and downward a certain pool of nutrients not being effectively used by the biology in the coastal areas. This process they called "nutrients leakage" is also having a negative feedback effect by diminishing the nutrients available in the deep waters being re-upwelled continuously.

In our work, we focused on the Benguela area, being the most contrasting area of all EBUS in term of mixing intensity. Although mechanisms involved occur in the 3D space, the initial observation of this suppressive effect was based only on two-dimensional (2D) datasets (Rossi et al., 2008). Here we use 2D numerical analysis in a simple semi-realistic framework to test the effect of horizontal advection versus biological dynamics. Meanwhile, since vertical dimension is crucial in upwelling areas, it was introduced in our model in a simplified way by considering a source term with an intensity and spatial distribution corresponding to the upwelling characteristics. Indeed other theoretical studies in idealized 2D settings display also negative correlation between mixing and biomass (Tél et al., 2005; MacKiver and Neufeld, 2009). Contrarily to EKE which is an Eulerian diagnostic tool, we used here a Lagrangian measurement of mesoscale intensity. It has been demonstrated as a powerful tool to study patchy chlorophyll distributions due to dynamical structures at mesoscale, such as upwelling filaments (Calil and Richards, 2010). Different velocity fields were considered, one obtained from satellite and others from numerical simulations. The robustness of our results with respect to spatial resolution is tested by using two numerical velocity datasets at different resolution. Our results are

compared with real distributions of chlorophyll (a metric for phytoplankton) obtained from SeaWiFS satellite.

This paper is organized as follows. In Sec. 2 we describe the different data sets for our analysis. Sec. 3 contains the methodology, including the Finite-Size Lyapunov exponents, and the plankton numerical model. Then, in Sec. 4 our results are presented and discussed in the context of existing bibliography. Finally in Sec. 5, we summed-up our main findings.

2. Satellite and simulated data.

A total of three sources of two-dimensional velocity data sets in the surface of the Benguela area were used: two were obtained from the numerical model ROMS (Regional Ocean Model System), and the other one from a combined satellite product. ROMS is a free surface, hydrostatic, primitive equation model, and the run used here was eddy resolving but climatologically forced (Gutknecht et al., 2011). At each grid point, linear horizontal resolution is the same in both the longitudinal, ϕ, and latitudinal, θ, directions, which leads to angular resolutions $\Delta\phi = \Delta_0$ and $\Delta\theta = \Delta\phi \cos\theta$. The numerical model was run onto 2 different grids: a coarse one at $\Delta_0 = 1/4^\circ$, and a finer one at $\Delta_0 = 1/12^\circ$ of spatial resolution. In the following we label the data set from the coarser resolution as *ROMS1/4*, and the finer one as *ROMS1/12*. In both of them, vertical resolution is variable with 30 layers in total. Only data from the upper layer were used. The third set of velocity data are surface currents computed from a combination of wind-driven Ekman currents, at 15 m depth, derived from Quickscat wind estimates, and geostrophic currents calculated using time variable Sea Surface Heights (SSH) obtained from satellite (Sudre and Morrow, 2008). These SSH were calculated from mapped altimetric sea level anomalies combined with a mean dynamic topography. This velocity field, labeled as *Satellite1/4*, covers a period from June 2002 to June 2005 with a spatial resolution of $\Delta_0 = 1/4^\circ$ in both longitudinal and latitudinal directions.

To validate simulated biological fields we used a three-year-long time series, from January 2002 to January 2005, of ocean color data. Phytoplankton pigment concentration (chlorophyll-a) are obtained from monthly SeaWiFS (Sea viewing Wide Field-of-view Sensor) products, generated by the NASA Goddard Earth Science (GES)/Distributed Active Archive Center (DAAC). Gridded global data were used with a resolution of approximately 9 by 9 km.

3. Methodology.

3.1. Finite Size Lyapunov Exponents (FSLEs).

FSLEs (Artale et al., 1997; Aurell et al., 1997; Boffetta et al., 2001) provides a measure of dispersion, and thus of stirring and mixing, as a function of the spatial resolution, serving to isolate the different regimes corresponding to different length scales of the oceanic flows, as well as identifying the Lagrangian Coherent Structures (LCSs) present in the data. FSLE are computed from τ, the time required for two particles of fluid (one of them placed at $\mathbf{x}$) to separate from an initial (at time t) distance of δ_0 to a final distance of δ_f, as

$$\lambda(\mathbf{x}, t, \delta_0, \delta_f) = \frac{1}{\tau} \log \frac{\delta_f}{\delta_0}. \tag{1}$$

It is natural to choose the initial points $\mathbf{x}$ on the nodes of a grid with lattice spacing coincident with the initial separation of fluid particles δ_0. Then, values of λ are obtained in a grid with lattice separation δ_0. In this work we take always the resolution of the FSLE field, δ_0, equal to the resolution of the velocity field, Δ_0. Other choices of parameter are possible and δ_0 can take any value, even much smaller than the resolution of the velocity field (Hernández-Carrasco et al., 2011a). This opens many possibilities that will not be explored in this work, since we focus here in the primary production, and, in some instances, the influence of the data resolution, not on the resolution of the FSLEs computation.

The field of FSLEs thus depends on the choice of two length scales: the initial, δ_0 and the final δ_f separations. As in previous works (d'Ovidio et al., 2004, 2009; Rossi et al., 2008; Hernández-Carrasco et al., 2011a) we will focus on transport processes at mesoscale, so that δ_f is taken as about 110 km, which is the order of the size of mesoscale eddies at mid latitudes. To compute λ we need to know the trajectories of the particles which gives Lagrangian character to this quantity. The equations of motion that describe the horizontal evolution of particle trajectories in longitudinal and latitudinal spherical coordinates, $\mathbf{x} = (\phi, \lambda)$, are:

$$\frac{d\phi}{dt} = \frac{u(\phi, \theta, t)}{R\cos\theta}, \tag{2}$$

$$\frac{d\theta}{dt} = \frac{v(\phi, \theta, t)}{R}, \tag{3}$$

where u and v represent the eastwards and northwards components of the surface velocity field, and R is the radius of the Earth (6400 km).

The ridges of the FSLE field can be used to define the Lagrangian Coherent Structures (LCSs) (Haller and Yuan, 2000; d'Ovidio et al., 2004, 2009; Tew Kai et al., 2009; Hernández-Carrasco et al., 2011a), useful to characterize the flow from the Lagrangian point of view (Joseph and Legras, 2002; Koh and Legras, 2002). In fact, since we are only interested in the ridges with large values of FSLE, the ones which significantly affect mixing, LCSs can be obtained as the regions with high values of FSLE, which have a line-like shape. We will compute FSLEs integrating backwards-in-time the particle trajectories, since attracting LCSs associated to this (the unstable manifolds) have a direct physical interpretation (Joseph and Legras, 2002; d'Ovidio et al., 2004, 2009). Tracers (chlorophyll, temperature, ...) spread along the attracting LCSs, thus creating their typical filamental structure (Lehan et al., 2007; Calil and Richards, 2010).

3.2. The Biological model

The plankton model is similar to the one used in previous studies by Oschlies and Garçon (1998, 1999) and Sandulescu et al. (2007, 2008). It describes the interaction of

a three-level trophic chain in the mixed layer of the ocean, including, phytoplankton P, zoo-plankton Z and dissolved inorganic nutrient N, whose concentrations evolve in time according to the following equations:

$$\frac{dN}{dt} = F_N = \Phi_N - \beta\frac{N}{\kappa_N + N}P + \mu_N\left((1-\gamma)\frac{\alpha\eta P^2}{\alpha+\eta P^2}Z + \mu_P P + \mu_z Z^2\right), \tag{4}$$

$$\frac{dP}{dt} = F_P = \beta\frac{N}{\kappa_N + N}P - \frac{\alpha\eta P^2}{\alpha+\eta P^2}Z - \mu_P P, \tag{5}$$

$$\frac{dZ}{dt} = F_Z = \gamma\frac{\alpha\eta P^2}{\alpha+\eta P^2}Z - \mu_Z Z^2. \tag{6}$$

where the dynamics of the nutrients, Eq. (4), is determined by nutrient supply due to the vertical mixing Φ_N, its uptake by phytoplankton (2^{nd} term) and its recycling by bacteria from sinking particles (3^{rd} term). Vertical mixing which brings nutrients from lower layers into the mixed surface layer of the ocean is parameterized in the model (see below), since the hydrodynamical part considers only horizontal 2D transport. Terms in Eq. (5) stand for phytoplankton growth by consuming N, the grazing by zooplankton, and its natural mortality. The last equation, Eq. (6), represents zooplankton growth by consuming phytoplankton minus its quadratic mortality.

A crucial part of this model comes in the vertical mixing, Φ_N, since it mimics the upwelling. Assuming constant nutrient concentration N_0 below the mixed layer, this term reads:

$$\Phi_N = S(\mathbf{x}, t)(N_0 - N), \tag{7}$$

where the temporally and spatially dependent (on the two dimension location $\mathbf{x}$) function S determines the strength and the horizontal spatial distribution of vertical mixing in the model, thus specifying the upwelling characteristics. Thus, the vertical dynamics is introduced in our two-dimensional model via this function S. Upwelling intensity along the coast is characterized by a number of cells of enhanced vertical ekman driven transport that are associated with similar fluctuations of the alongshore wind (Demarcq et al., 2003; Veitch et al., 2009). Following these results, we use a function S which is different from

zero in a strip 0.5° wide from the coast. Its spatial dependence along the coast is plotted in Fig. 1. For the temporal dependence, S alternates between the two configurations displayed in Fig. 1 one for winter and another for summer. Six separate upwelling cells can be discerned in the figure, with peaks at approximately 33°S, 31°S, 27.5°S, 24.5°S, 21.5°S, 17.5°S, which are known with the following names: Peninsula, Columbine+Namaqua, Luderitz, Walvis Bay, Namibia and Cunene, respectively. Luderitz being the strongest.

The dynamical system given by Eqs. (4,5,6), for values of S in the range shown on Fig. 1, evolves towards equilibrium for N, P and Z. But S is not fixed and its spatial dependence introduces a coupling with the hydrodynamics. The transient time to reach equilibrium is typically 60 days with the initial concentrations used (see Sec. 3.3). The parameters are set following a study by Pasquero et al. (2004) and are listed in Table 1.

parameter	value
β	0.66 day^{-1}
η	1.0 $(\text{mmol N m}^{-3})^{-2}$ day^{-1}
γ	0.75
a	2.0 day^{-1}
k_N	0.5 mmol N m^{-3}
μ_N	0.2
μ_P	0.03 day^{-1}
μ_Z	0.2 $(\text{mmol N m}^{-3})^{-2}$ day^{-1}
N_0	8.0 mmol N m^{-3}

Table 1: List of parameters used in the biological model.

3.3. Coupling hydrodynamical and biological model in Benguela.

The evolution of the concentrations within a flow is determined by the coupling between the hydrodynamical and biological models, and it is performed by the advection-

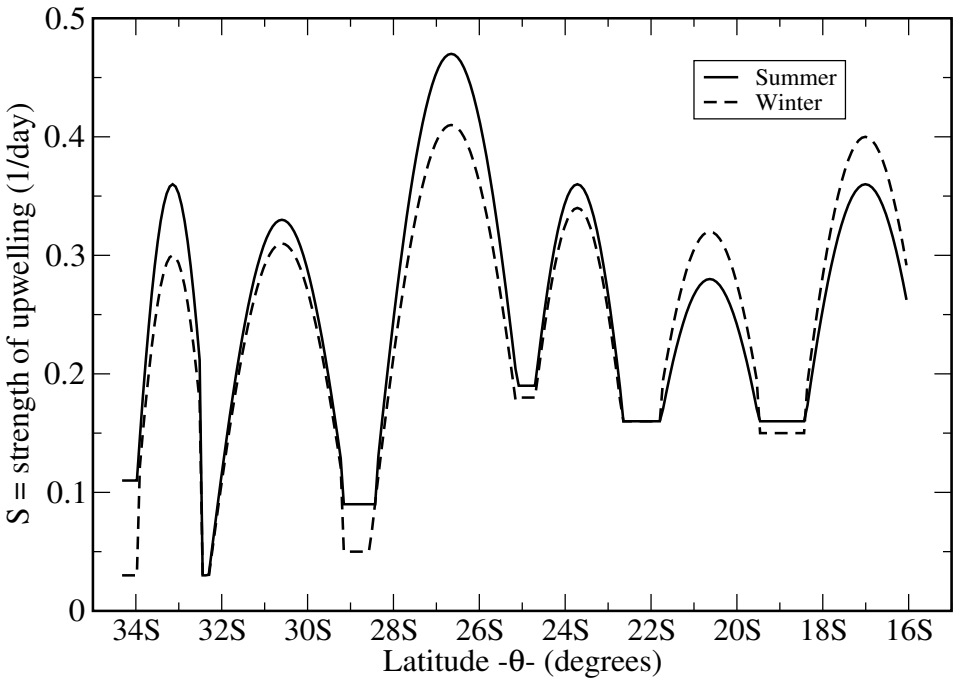

Figure 1: Shape and values of the strength (S) of the upwelling cells used in the simulations for winter and summer seasons (following Veitch et al. (2009)).

reaction-diffusion system. Thus, the complete model is given by the following system of partial differential equations:

$$\frac{\partial N}{\partial t} + \mathbf{v}\nabla N = F_N + D\nabla^2 N, \tag{8}$$

$$\frac{\partial P}{\partial t} + \mathbf{v}\nabla P = F_P + D\nabla^2 P, \tag{9}$$

$$\frac{\partial Z}{\partial t} + \mathbf{v}\nabla Z = F_Z + D\nabla^2 Z. \tag{10}$$

The biological model is the one described before by the functions F_N, F_P and F_Z. Horizontal advection is the 2D velocity $\mathbf{v}$, which is obtained from satellite data or from

the ROMS model. We add also an eddy diffusion term, via the ∇^2 operator, acting on N, P, and Z to incorporate the small-scale turbulence, which is not explicitly taken into account by the velocity fields used.

The eddy diffusion coefficient, D, is given by Okubo's formula (Okubo, 1971), $D(l) = 2.055 * 10^{-4}\ l^{1.15}$, where l is the value of the resolution, in meters, corresponding to the angular resolution $l = \Delta_0$. The formula gives the values D=26.73 m^2/s for *Satellite1/4* and *ROMS1/4*, and D=7.4 m^2/s for *ROMS1/12*.

The coupled system Eqs. (8,9,10) is solved numerically by the semi-Lagrangian algorithm described in Sandulescu et al. (2007), combining Eulerian and Lagrangian schemes. The initial concentrations of the tracers were taken from Koné et al. (2005) and they are $N_0 = 1\ mmolNm^{-3}$, $P_0 = 0.1\ mmolNm^{-3}$, and $Z_0 = 0.06\ mmolNm^{-3}$. The inflow conditions at the boundaries are specified in the following way: into the eastern, western, and southern parts of the computation domain fluid parcels enter with very poor biomasses concentration: $N_L = 0.01N_0\ mmolNm^{-3}$, $P_L = 0.01P_0\ mmolNm^{-3}$, and $Z_L = 0.01Z_0\ mmolNm^{-3}$. Across the northern boundary, fluid parcels enter with higher concentrations $N_H = 5\ mmolNm^{-3}$, $P_H = 0.1\ mmolNm^{-3}$, and $Z_H = 0.06\ mmolNm^{-3}$ according with the values given by CARS for the Benguela system (Condie and Dunn, 2006). The integration time step is $dt = 6$ hours.

4. Results and discussion.

In this section we first compute the FSLEs on the velocity fields to quantify the horizontal stirring activity over the area. Then we analyze the results of the coupled biological-hydrodynamic model. Finally we investigate the relation between horizontal stirring activity and biological productivity.

4.1. Horizontal activity

We have computed the FSLE with a initial separation of particles equal to the spatial resolution of each velocity fields (δ_0= 1/4° for *Satellite1/4* and *ROMS1/4*, and δ_0= 1/12°

for *ROMS1/12*). As already mentioned, the final distance is always chosen to focus on transport processes by mesoscale structures at mid latitudes, $\delta_f = 1°$. The areas of more intense horizontal mixing can be identified using time averages of the backward FSLEs (d'Ovidio et al., 2004). Figure 2 allows an easy characterization of sub-regions with different horizontal mixing activity in the Benguela system. Areas of large average values of FSLEs are identified as exhibiting an intense horizontal stirring or mesoscale activity. We confirm the results of Rossi et al. (2009) by using different velocity data sets. Although there are visible differences in the detailed patterns, good agreement between all datasets is shown when computing the spatial correlation: for instance, correlation coefficient R^2 between FSLEs map from *Satellite1/4* and from *ROMS1/4* is 0.81. Correlation coefficients between *Satellite1/4* and *ROMS1/12* on one hand, and between *ROMS1/4* and *ROMS1/12* on the other hand, are lower (0.61 and 0.77 respectively) since the FSLE were computed on a different resolution. More details on the effect on the grid resolution when computing FSLEs can be found in Hernández-Carrasco et al. (2011a). For all data sets high mixing values are observed in the southern region, while the northern area displays significantly lower values. Note that the separation is well marked for *Satellite1/4* where the line between the two areas is around 27°. In the case of the ROMS data sets, the mixing activity is more homogeneously distributed, although the north-south gradient is still present. We associate this difference with the injection of strong and numerous Agulhas rings into the south of the area from the Agulhas retroflection.

The latitudinal behavior of mixing along the coastal upwelling can be seen in Fig. 3. This was performed by computing the longitudinal averages of the plots in Fig. 2 for two coastally oriented strips, of 3° and 6° width, respectively. It is clear that horizontal mixing decreases as latitude decreases. Note that there are differences in the mixing values (FSLEs) depending on the type of data, their resolution and the grid size of FSLE computation. In general, considering velocities with the same resolution, the lower values correspond to *Satellite1/4* as compared to *ROMS1/4*. On average, values of mixing from

ROMS1/4 are larger than those from *ROMS1/12*, whereas we would expect the opposite considering the higher resolution of the latter simulation favouring small scales processes. However a caveat here is that FSLE were not computed on the same resolution, so there are not directly comparable. Note also that a low-mixing region is observed from 28° to 30°S on all calculations. It seems to indicate that the ROMS model is representing pretty well the spatial variability of the mixing. As proposed in a recent study by Titaud et al. (2011), these preliminary results indicate that FSLEs could be used as a diagnostic to validate eddy-resolving oceanic models.

In Fig. 3 (bottom) we see that, for *Satellite1/4*, the values of FSLEs decay from 0.18 $days^{-1}$ in the southern to 0.03 $days^{-1}$ in the northern area, with similar decays for *ROMS1/4*. Specifically the North-South difference for *Satellite1/4*, *ROMS1/4* and *ROMS1/12* are of the order of 0.15 $days^{-1}$, 0.15 $days^{-1}$ and 0.08 $days^{-1}$, respectively, confirming a lower latitudinal gradient for the case of *ROMS1/12*. These values do not change much when it is averaged over the 3 degrees stripe offshore (Fig. 3, top), although in this case relative maxima and minima appear, probably in relation with the complex and variable shelf circulation.

The mixing behavior can be also assessed by looking at a proxy of the intensity of mesoscale activity, the Eddy Kinetic Energy (EKE), as done in Gruber et al. (2011). Fig. 4 shows that there are regions, as in the FSLE case, with distinct dynamical characteristics. Larger values appear in the south and smaller in the north. This distribution is in good agreement with the one deducted from the FSLEs (Fig. 2). Some simple spatial correlation (not shown) indicate that EKE and FSLE patterns are well correlated when using a non-linear fitting (power law). For instance, EKE and FSLE computed on the velocity field from *Satellite1/4* exhibit a R^2 of 0.86 for the non-linear fitting: $FSLE = 0.009 \cdot EKE^{0.49}$. It is in agreement with the initial results from Waugh et al. (2006); Waugh and Abraham (2008), for a related dispersion measurement, and confirmed the thorough investigation of the relationship between EKE and FSLE by Hernández-Carrasco et al. (2011b).

In the following sections, we study the effect of this variable surface mixing activity on the plankton dynamics.

4.2. Plankton dynamics in the Benguela upwelling system.

Evolution of N, P and Z over space and time is obtained by integrating the systems described by Eqs. 8,9,10. The biological model is coupled to the velocity field after the transient time needed to reach stability (60 days). In Fig.5 we show some snapshots of phytoplankton concentrations for the three velocity fields at different times. Since both ROMS simulation were climatologically forced runs, the dates do not correspond to a specific year, whereas we used the actual date for *Satellite1/4*. The most relevant feature is the larger value of concentrations near the coast due to the injection of nutrients following Fig. 1. Obviously the spatial distribution of P is dominated by the submeso- and meso-scale structures such as filaments and eddies. This is specially noticeable in the south, due to the presence of several Agulhas rings, cyclonic eddies and filaments. Differences are however observed for the three data sets. In particular, it seems that for *Satellite1/4* and *ROMS1/12* the concentrations extend farther offshore than for *ROMS1/4*.

Several studies (Lehan et al., 2007; d'Ovidio et al., 2009; Calil and Richards, 2010) have shown that chlorophyll distributions in the marine surface are linked to the local maxima or ridges of the FSLEs. This also occurs in our numerical setting, as it is visually shown in Fig. 6. We superimpose contours of high values of FSLE (locating the LCS) on top of phytoplankton concentrations for *ROMS1/12* (every 8 days during a 32 days period). In some regions P concentrations are constrained and stirred by lines of FSLE. For instance, the edges of the cyclonic and anti-cyclonic eddies centered at 6 °E, 32 °S, and 28 °S in Fig. 6 on June 11 exhibit large values of phytoplankton concentration. This reflects the fact that tracers, even active such as chlorophyll, still disperse along these LCSs.

In order to reveal regions of more intense biological activity, we have computed the temporal average of simulated P. The results, plotted in Fig.7 a), b), c), show that

coastal regions with high P extend approximately, depending on latitude, between half a degree and two degrees offshore. It is comparable with the pattern obtained from the satellite-derived chlorophyll data (Fig.7 d)). The spatial correlation of averaged simulated chlorophyll with satellite is as follows: $R^2 = 0.85$ for *Satellite1/4* versus *SeaWIFS*; $R^2 = 0.89$ for *ROMS1/4* versus *SeaWIFS* and $R^2 = 0.85$ for *ROMS1/12* versus *SeaWIFS*. Despite the very simple setting of our models, the phytoplankton development over the Benguela shelf is well simulated by the upwelling parameterization chosen. Note however that our simulated chlorophyll values are about $\simeq$ 3-4 times lower than satellite data, as shown by the colorbar scale. Of course several factors, both biological and physical, are not taken into account in this simple setting that might explain this offset. Another possible explanation is the low reliability of the ocean color in very coastal waters optically complex.

We now examine the latitudinal distribution of P. The top row in Fig.8 displays the outputs of the numerical simulations that were averaged over a coastal strip of 3° (left) and 6° (right) width. The bottom row is the same but from the satellite chlorophyll data. First of all, phytoplankton biomass has a general tendency to decrease with latitude, an opposite tendency to the ones exhibited by mixing (from FSLEs and EKE) for the three data sets. P values are higher in the northern than in the southern area of Benguela. A common feature is the minimum located just below the Luderitz upwelling cell (28°S), maybe related to the presence of a physical boundary, already studied and named the LUCORC barrier by Shannon et al. (2006) and Lett et al. (2007). Note that on Fig. 3 (upper plot), the same latitude was marked by a local maximum of mixing that might be responsible for this barrier. Though not so evident, the same latitudinal tendency is observed for the SeaWIFS data plotted in Fig. 8c) and d). Correlation of zonal average of simulated chlorophyll versus satellite data does not give striking results when considering the whole area (R^2 ranging from 0.1 to 0.5). However, when considering each subsystem independently, high correlation coefficients are found for the south Benguela (R^2 around

0.75), but not for the north. It clearly indicates that our simple modelling approach is able tostimulate well the spatial patterns of chlorophyll in the south Benguela, but not properly in the northern part. The 2D vigorous mixing in the south and its associated intense offshore export are sufficient to explain reasonable latitudinal patterns of P. The numerous eddies released from the Agulhas system, moving offshore in the south Benguela, might limit the large development of P by exporting unused nutrients and young phytoplankton communities toward the open ocean, as stated by Gruber et al. (2011). It also suggests that the negative effect seems to be mainly driven by 2D advection toward the open ocean. In the north, other factors seem to play an important role. Among many others, the 3D flow, the shelf width, the rivers and aeolian inputs, the remineralisation pattern, the presence of particular biogeochemical functioning,...etc. have been disregarded from this study, whereas they seem to impact widely plankton dynamics in the north.

To address the question of the negative effect of horizontal stirring on phytoplankton concentration in a more quantitative way, we have examined the correlation between these two quantities. We have plotted spatial averages over each subregion (North and South) of every weekly map of FSLE versus the same average of the corresponding weekly map of P, for each week during three years in the case of Satellite and for one year for the case of ROMS (Fig.9). For all cases, a negative correlation between FSLEs and chlorophyll emerges. Thus, the higher the surface stirring/mixing, the lower the biomass concentration. The correlation coefficient is quite similar for all the plots (R^2=0.80 to 0.84), and the slopes have the following values: -1 for *Satellite1/4*, -0.65 for *ROMS1/4* and -1.5 for *ROMS1/12*. Note that, similarly to the results of Rossi et al. (2008, 2009) and Gruber et al. (2011), the negative slope is larger but less robust when considering the whole area rather than within every subregion. The suppressive effect of mixing might be dominant only when mixing is intense, as in the south Benguela. Moreover, Gruber et al. (2011) stated that the reduction of biomass due to eddies may extend beyond the regions of the most intense mesoscale activity, not considered here. In fact in our simulations, we

observe than averaging FSLEs over a 3° or a 6° coastal band returns quite comparable absolute values, attesting of a significant mixing spreading offshore. However average values of P in Fig. 8 decrease when averaging over a wider area.

The same inverse relationship is observed in Fig.10 using chlorophyll data from SeaWIFS. This analysis confirms the result obtained from satellite velocity fields by Rossi et al. (2008, 2009) but using FSLEs computed on simulated velocity field with ROMS, at two different resolutions. In this case, the value of the slopes are: -3.5, -3.4 and -4.7 for *Satellite1/4*, *ROMS1/4* and *ROMS1/12*, respectively. The fact that ROMS velocity data do not necessarily match the dates of SeaWIFS may explain the larger discrepancy in the values of the correlation coefficient showed in Fig.10.

Then, let us present a brief description of the seasonal behavior of the system. In Fig. 11 we display the temporal evolution over one year of the spatial averages of FSLEs (upper plot) and P (bottom). A climatological average for the case of *Satellite1/4* using three years of data. We observe that the seasonal increase in mixing activity (from May to September, roughly winter) is associated to a decrease of the simulated phytoplankton. This also illustrates the seasonal inhibiting effect that the mixing activity has on the phytoplankton dynamics in winter. Note that the seasonal variation of light is not taken into account in our model. However, the temporal variability of plankton in the Benguela is mainly driven by the varying activity of the coastal upwelling cells, reproduced by the function S.

Finally, a few sensitivity analysis were done to clarify the role of the 2D advection and the biological reactions in the simulated plankton fields. For this, we performed virtual experiments to determine the effect of both processes taken separately. A simulation with only advection of a passive tracer (without any upwelling parameterization) is compared to a similar simulation adding the biological reaction terms. The advection-only case reproduces well the smaller tracer concentrations in the southern domain, whereas the advection-reaction case presents a more constant latitudinal profile (see Fig. 12). This

confirms that the main influence on the spatial distribution of phytoplankton in the south is 2D advection, with the biological dynamics playing a minor role.

Also, the per capita growth rate of N over time (i.e. $N^{-1}dN/dt$) was computed and averaged over the coastal area in each subsystem to test the mechanisms proposed by Gruber et al. (2011) (see Fig. 13 for the *ROMS1/12* simulation). We found that the mean value for each subsystem, North and South, are $-3 \cdot 10^{-5}$ and $-1 \cdot 10^{-4}$ day^{-1}, respectively. This confirms that nutrients are being lost toward the open ocean by simple 2D advection almost four times more in the south than in the north. It has to be compared with the mixing activity being about three times higher in the south than in the north (Fig. 3). The same behavior is also observed in the other two cases *ROMS1/4* and *Satellite* (not shown). Note also that the loss of nutrient appear to be maximal in the winter months (maximum mixing), although there is a slight decay in between the two subsystems.

5. Conclusions

This study is based on numerical analysis from a simple biological NPZ model coupled with different velocity fields (satellite and model) over the Benguela area. Although in a simple framework, a reduction of phytoplankton concentrations in the coastal upwelling for increasing mesoscale activity has been successfully simulated. Horizontal stirring was estimated by computing the FSLEs and was correlated negatively with chlorophyll stocks. Similar results are found, though not presented in this manuscript, for the primary production, defined as the first term in F_P (Eq.5), i.e. $PP = \beta \dfrac{N}{\kappa_N + N} P$. Some recent observational and modelling studies proposed the "nutrient leakage" as a mechanism to explain this negative correlation. Here we argue that Lagrangian Coherent Structures, mainly mesoscale eddies and filaments, transport a significant fraction of the recently upwelled nutrients nearshore toward the open ocean before being efficiently used by the pelagic food web. Although some studies dealt with 3D effect, we have shown that 2D

advection processes seems to play an important role in this suppressive effect. Our analysis suggest that the inhibiting effect of the mesoscale activity on the plankton occurs when the mixing reach high levels, as in the south Benguela. However, this effect is not dominant under certain levels of turbulence. We have also shown that the inhibiting effect of intense mixing is maximal during the winter months. It might indicate that planktonic ecosystems in oceanic regions with vigorous mesoscale dynamics can be, as a first approximation, easily modeled just by including a realistic flow field. The small residence times of waters in the productive area will smooth out all the other neglected biological factors in interaction. However, these factors are required when modelling an oceanic regions with low mixing, associated with high residence time leading to the predominance of complex combinations of factors.

Our findings confirm the unexpected role that mesoscale activity has on biogeochemical dynamics in the productive coastal upwelling. Strong vertical velocities are known to be associated with these physical structures and they might have another direct effect by transporting downward rich nutrient waters below the euphotic zone. Further studies are needed such as 3D realistic modelling that take into account the strong vertical dynamics in upwelling regions to test the complete mechanisms involved.

Acknowledgments

I.H-C was awarded a FPI grant from MICINN to visit LEGOS. V.R thanks funding from OCEANTECH project (CSIC PIF-2006) to visit IFISC. V.R. was partly supported by a DGA grant and an Australian Research Council Grant DP1093510 while finishing this work. I.H-C, C.L and E.H-G acknowledge support from MICINN and FEDER through project FISICOS (FIS2007-60327) and of CSIC through TURBID and OCEANTECH. V. G. thanks CNES funding through Hiresubcolor project. We are also grateful to J. Sudre for providing us velocity data sets both from ROMS and from the combined satellite product. Ocean color data were produced by the SeaWiFS project at GES and were

obtained from DAAC.

References

Artale, V., Boffetta, G., Celani, A., Cencini, M., Vulpiani, A., 1997. Dispersion of passive tracers in closed basins: Beyond the diffusion coefficient. Phys. Fluids 9, 3162–3171.

Aurell, E., Boffetta, G., Crisanti, A., Paladin, G., Vulpiani, A., 1997. Predictability in the large: an extension of the Lyapunov exponent. J. Phys. A 30, 1–26.

Boffetta, G., Lacorata, G., Redaelli, G., Vulpiani, A., 2001. Detecting barriers to transport: a review of different techniques. Physica D 159, 58–70.

Brink, K., Cowles, T., 1991. The coastal transition zone program. J. Geophys. Res 14, 637–647.

Calil, P., Richards, K., 2010. Transient upwelling hot spots in the oligotrophic North Pacific. J. Geophys. Res 115, C02003.

Condie, S., Dunn, J. R., 2006. Seasonal characteristics of the surface mixed layer in the Australasian region: implications for primary production regimes and biogeography Marine and Freshwater Research. Marine and Freshwater Research 57, 1–22.

Correa-Ramirez, M., Hormazabal, S., Yuras, G., 2007. Mesoscale eddies and high chorophyll concentrations off central Chile (29°S - 39°S). Geophys. Res. Lett 34, L12604.

Demarcq, H., Barlow, R., Shillington, F., 2003. Climatology and variability of sea surface temperature and surface chlorophyll in the Benguela and Agulhas ecosystems as observed by satellite. African Journal of Marine Science 25, 363–372.

d'Ovidio, F., Fernández, V., Hernández-García, E., López, C., 2004. Mixing structures in the Mediterranean sea from finite-size Lyapunov exponents. Geophys. Res. Lett. 31, L17203.

d'Ovidio, F., Isern-Fontanet, J., López, C., Hernández-García, E., García-Ladona, E., 2009. Comparison between Eulerian diagnostics and Finite-Size Lyapunov Exponents computed from altimetry in the Algerian basin. Deep-Sea Res. I 56, 15–31.

Gruber, N., Lachkar, Z., Frenzel, H., Marchesiello, P., Münnich, M., McWilliams, J., Nagai, T., Plattner, G., 2011. Eddy-induced reduction of biological production in eastern boundary upwelling systems. Nature Geoscience 9, 787–792.

Gutknecht, E., Dadou, I., Cambon, B. L. V. G., Sudre, J., Garçon, V., Machu, E., Rixen, T., Kock, A., Flohr, A., Paulmier, A., Lavik, G., 2011. Nitrogen transfers and air-sea N2O fluxes in the upwelling off Namibia within the oxygen minimum zone: a 3-d model approach. Biogeosciences Discuss 8, 3537–3618.

Haller, G., Yuan, G., 2000. Lagrangian coherent structures and mixing in two-dimensional turbulence. Physica D 147, 352–370.

Hernández-Carrasco, I., López, C., Hernández-García, E., Turiel, A., 2011a. How reliable are finite-size Lyapunov exponents for the assesment of ocean dynamics? Ocean Modelling 36(3-4), 208–218.

Hernández-Carrasco, I., López, C., Hernández-García, E., Turiel, A., 2011b. Seasonal and regional characterization of horizontal mixing in the global ocean. Preprint available from arXiv:1103.5927v2.

Hutchings, L., van der Lingen, C., Shannon L.J. Crawford, R., Verheye, H., Bartholomae, C., van der Plas, A., Louw, D., Kreiner, A., Ostrowski, M., Fidel, Q., Barlow, R., Lamont, T., Coetzee, J., Shillington, F., Veitch, J., Currie, J., Monteiro, P., 2009. The Benguela Current: An ecosystem of four components. Progress in Oceanography 83, 15–32.

Joseph, B., Legras, B., 2002. Relation between Kinematic Boundaries, Stirring, and Barriers for the Antartic Polar Vortex. J. Atm. Sci. 59, 1198–1212.

Koh, T., Legras, B., 2002. Hyperbolic lines and the stratospheric Polar vortex. Chaos 12 (2), 382–394.

Koné, V., Machu, E., Penven, P., Andersen, V., Garçon, V., Fréon, P., Demarcq, H., 2005. Modeling the primary and secundary productions of the southern Benguela upwelling system: A comparative study through two biogeochemical models. Global Biogeochem. Cycles 19, GB4021.

Lehan, Y., d'Ovidio, F., Lévy, M., Heyfetz, E., 2007. Stirring of the Northeast Atlantic spring bloom: A Lagrangian analysis based on multisatellite data. J. Geophys. Res. 112, C08005.

Lett, C., Veitch, J., van der Lingen, C., Hutchings, L., 2007. Assessment of an environmental barrier to transport of ichthyoplankton from the southern to the northern Benguela ecosystems. Marine Ecology Progress Series 347, 247–259.

Mackas, D., Strub, P., Thomas, C., Montecino., V., 2006. Eastern ocean boundaries pan-regional view. In: Robinson, A., Brink, K. (Eds.), The Sea, vol 14a, The global Coastal Ocean: Interdisciplinary Regional Studies and Syntheses: Pan-Regional Syntheses and the Coast of North and South America and Asia. Harvard Univ. Press, chap. 2, Cambridge, Mass.

MacKiver, W., Neufeld, Z., 2009. The influence of turbulent advection on a phytoplankton ecosystem with non-uniform carrying capacity. Phys. Rev. E. 79, 061902.

Martin, A., 2003. Phytoplankton patchiness: the role of lateral stirring and mixing. Progress in Oceanography 57, 125–174.

McGillicuddy, D., Anderson, N., Bates, T., Buesseler, K., 2007. Eddy/wind interactions stimulate extraordinary mid-ocean plankton blooms. Science 316, 1021–1026.

494 Monteiro, P., 2009. Carbon fluxes in the Benguela upwelling system. In: Liu, K., Atkin-
495 son, L., Quiñones, R., Talaue-McManus, L. (Eds.), Carbon and Nutrient Fluxes in
496 Continental Margins: A global Synthesis, Chap. 2. Springer, Berlin.

497 Okubo, A., 1971. Oceanic diffusion diagrams. Deep-Sea Res. 18, 789–802.

498 Oschlies, A., Garçon, V., 1998. Eddy-induced enhancement of primary productivity in a
499 model of the North Atlantic Ocean. Nature 394, 266–269.

500 Oschlies, A., Garçon, V., 1999. An eddy-permitting coupled physical-biological model of
501 the North Atlantic, sensitivity to advection numerics and mixed layer physics. Global
502 Biocheochem. Cycles 13, 135–160.

503 Pasquero, C., Bracco, A., Provenzale, A., 2004. Coherent vortices, Lagrangian parti-
504 cles and the marine ecosystem. In: Uijttewaal, W., Jirka, G. (Eds.), Shallow Flows.
505 Balkema, Leiden.

506 Rossi, V., López, C., Hernández-García, E., Sudre, J., Garçon, V., Morel, Y., 2009. Sur-
507 face mixing and biological activity in the four Eastern Boundary Upwellings Systems.
508 Nonlinear Process. Geophys. 16, 557–568.

509 Rossi, V., López, C., Sudre, J., Hernández-García, E., Garçon, V., 2008. Comparative
510 study of mixing and biological activity of the Benguela and Canary upwelling systems.
511 Geophys. Res. Lett. 35, L11602.

512 Sandulescu, M., Hernández-García, E., López, C., Feudel, U., 2007. Plankton blooms
513 in vortices: the role of biological and hydrodynamics timescales. Nonlinear Process.
514 Geophys. 14, 443–454.

515 Sandulescu, M., López, C., Hernández-García, E., Feudel, U., 2008. Biological activity in
516 the wake of an island close to a coastal upwelling. Ecological Complexity 5, 228–237.

Shannon, L., Hempel, G., Malanotte-Rizzoli, P., Moloney, C., Woods, J. (Eds.), 2006. Benguela: Predicting a Large Marine Ecosystem. Elsevier.

Sudre, J., Morrow, R., 2008. Global surface currents: a high resolution product for investigating ocean dynamics. Ocean Dyn. 58(2), 101–118.

Tél, T., de Moura, A., Grebogi, C., Károlyi, G., 2005. Chemical and biological activity in open flows: A dynamical system approach. Physics Reports 413, 91–196.

Tew Kai, E., Rossi, V., Sudre, J., Weimerskirch, H., López, C., Hernández-García, E., Marsac, F., Garçon, V., 2009. Top marine predators track Lagrangian coherent structures. Proceedings of the National Academy of Sciencies of the USA 106, 8245–8250.

Titaud, O., Brankart, J. M., Verron, J., 2011. On the use of Finite-Time Lyapunov Exponents and Vectors for direct assimilation of tracer images into ocean models. Tellus A 63, 1038–1051.

Veitch, J., Penven, P., Shillington, F., 2009. The Benguela: A laboratory for a comparative modeling studies. Progress in Oceanography 83(1-4), 296–302.

Waugh, D. W., Abraham, E. R., 2008. Stirring in the global surface ocean. Geophys. Res. Lett. 35, L20605.

Waugh, D. W., Abraham, E. R., Bowen, M. M., 2006. Spatial variations of stirring in the surface ocean: A case of study of the Tasman sea. J. Phys. Oceanogr. 36, 526–542.

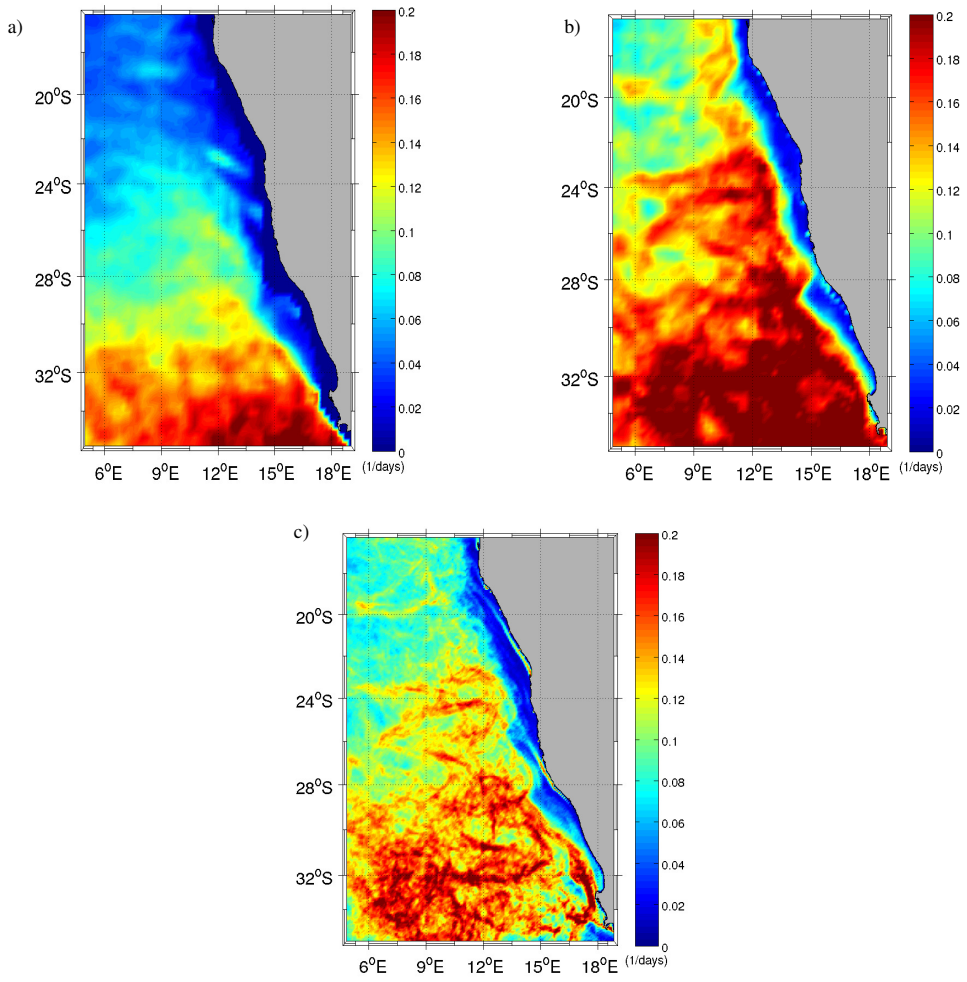

Figure 2: Spatial distribution of time average of weekly FSLE maps in the Benguela region. a) Three years average using data set *Satellite1/4*; b) one year average using *ROMS1/4*; c) one year average using *ROMS1/12*. The units of the colorbar are $1/days$.

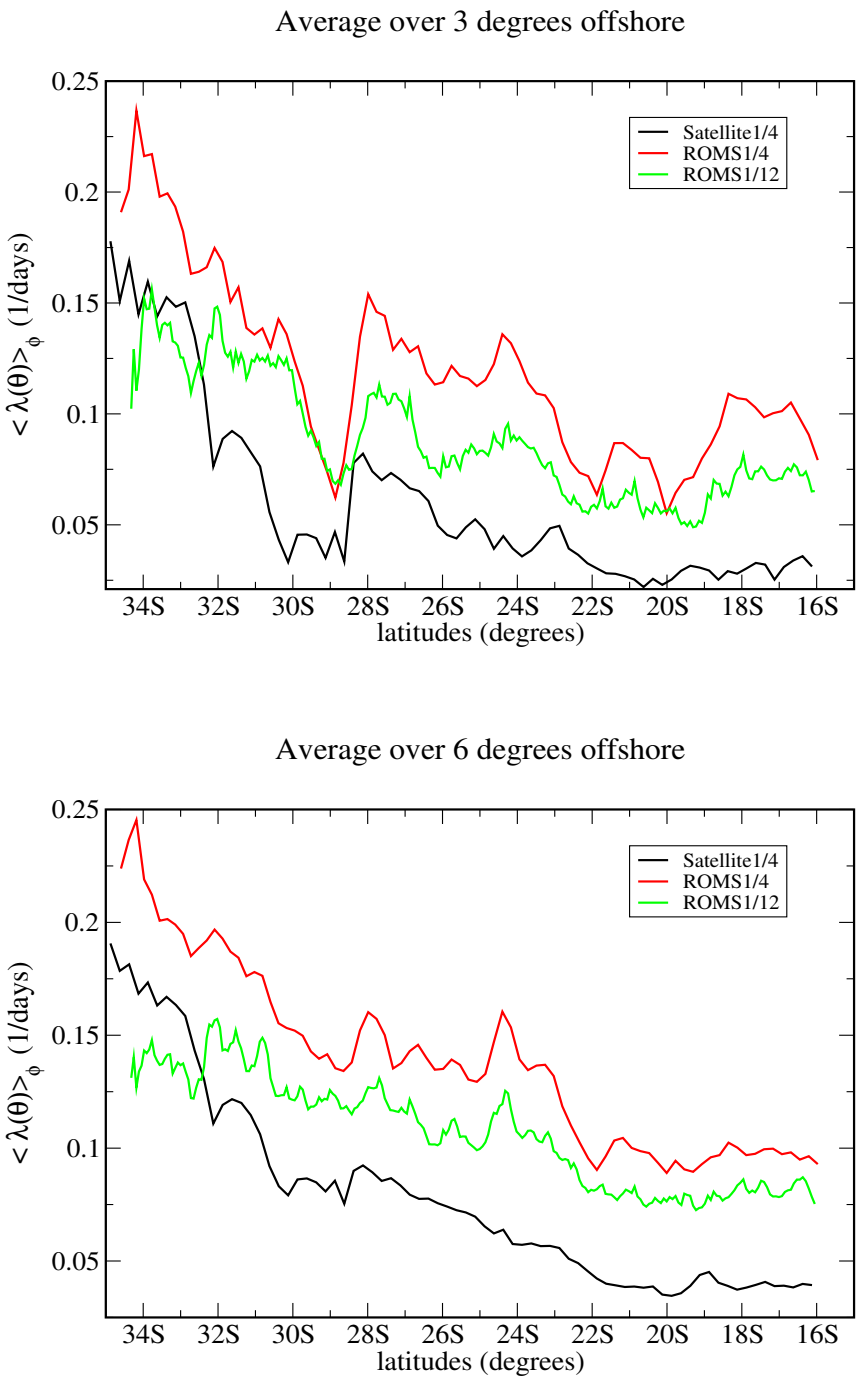

Figure 3: Zonal average over coastal bands of the FSLE time averages from Fig. 2 as a function of latitude. Top) From the coast to 3 degrees offshore; bottom) to 6 degrees offshore.

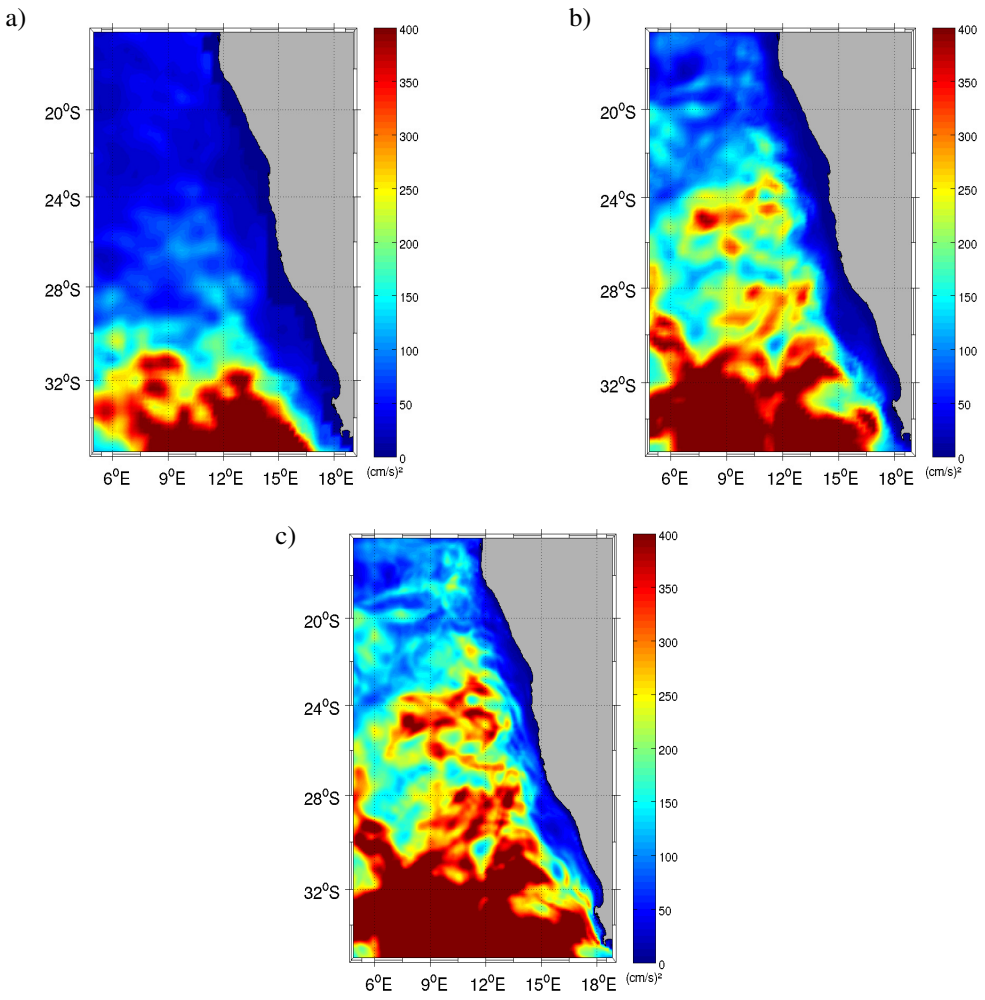

Figure 4: Spatial distribution of annual EKE in the Benguela region. a) using velocity data from Satellite at spatial resolution 1/4° (*Satellite1/4*) b) using velocity data from ROMS at spatial resolution 1/4° (*ROMS1/4*) c) using velocity data from ROMS at spatial resolution 1/12° (*ROMS1/12*). The units of the colorbar are $(cm/s)^2$

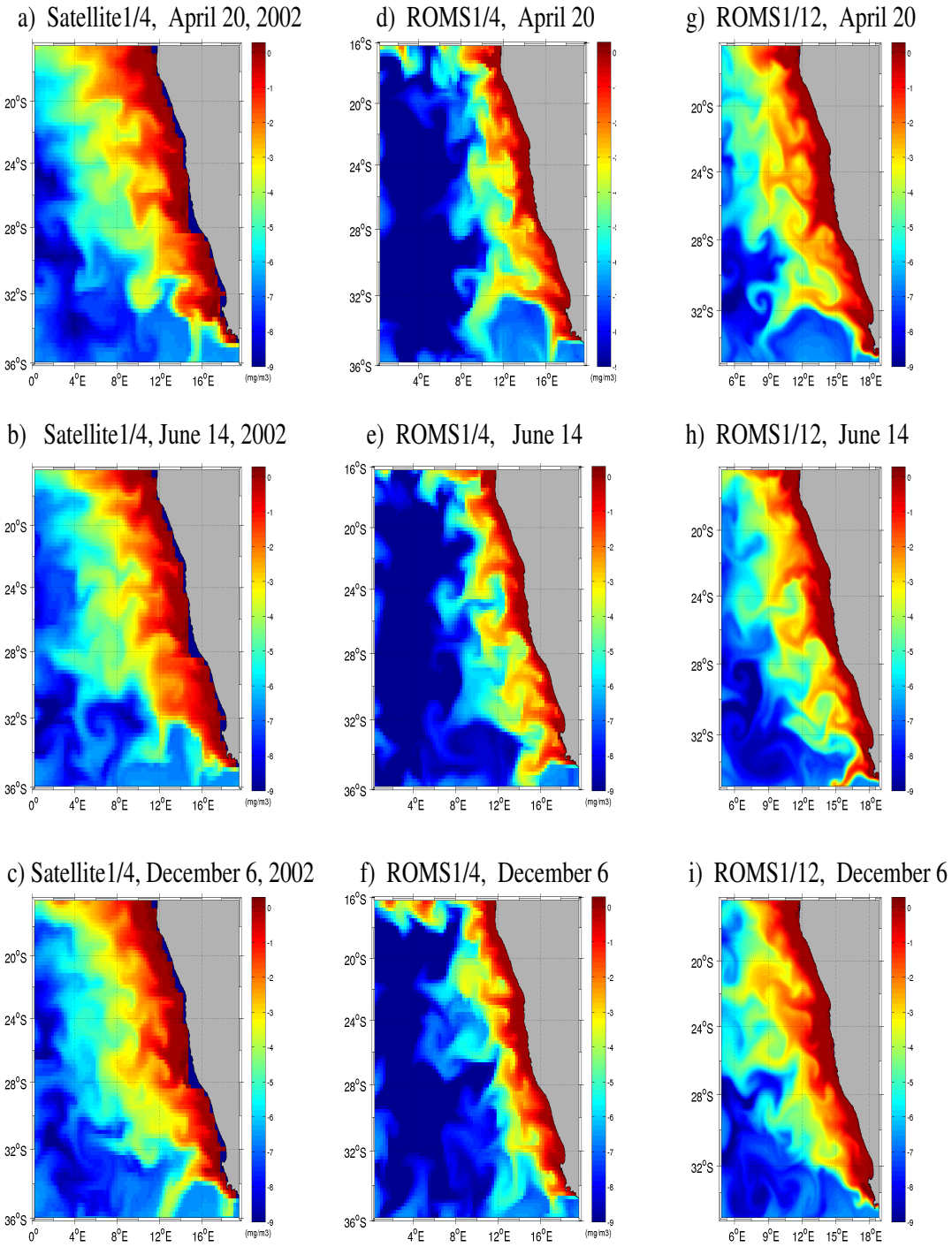

Figure 5: Snapshots of spatial distribution of phytoplankton concentration from the simulations: Left column) corresponding to the simulation using *Satellite1/4* ; Middle column) *ROMS1/4*; Right column) from *ROMS1/12*. Logarithmic scale is used to improve the visualization of the structures. The units for the colorbar are mg/m^3

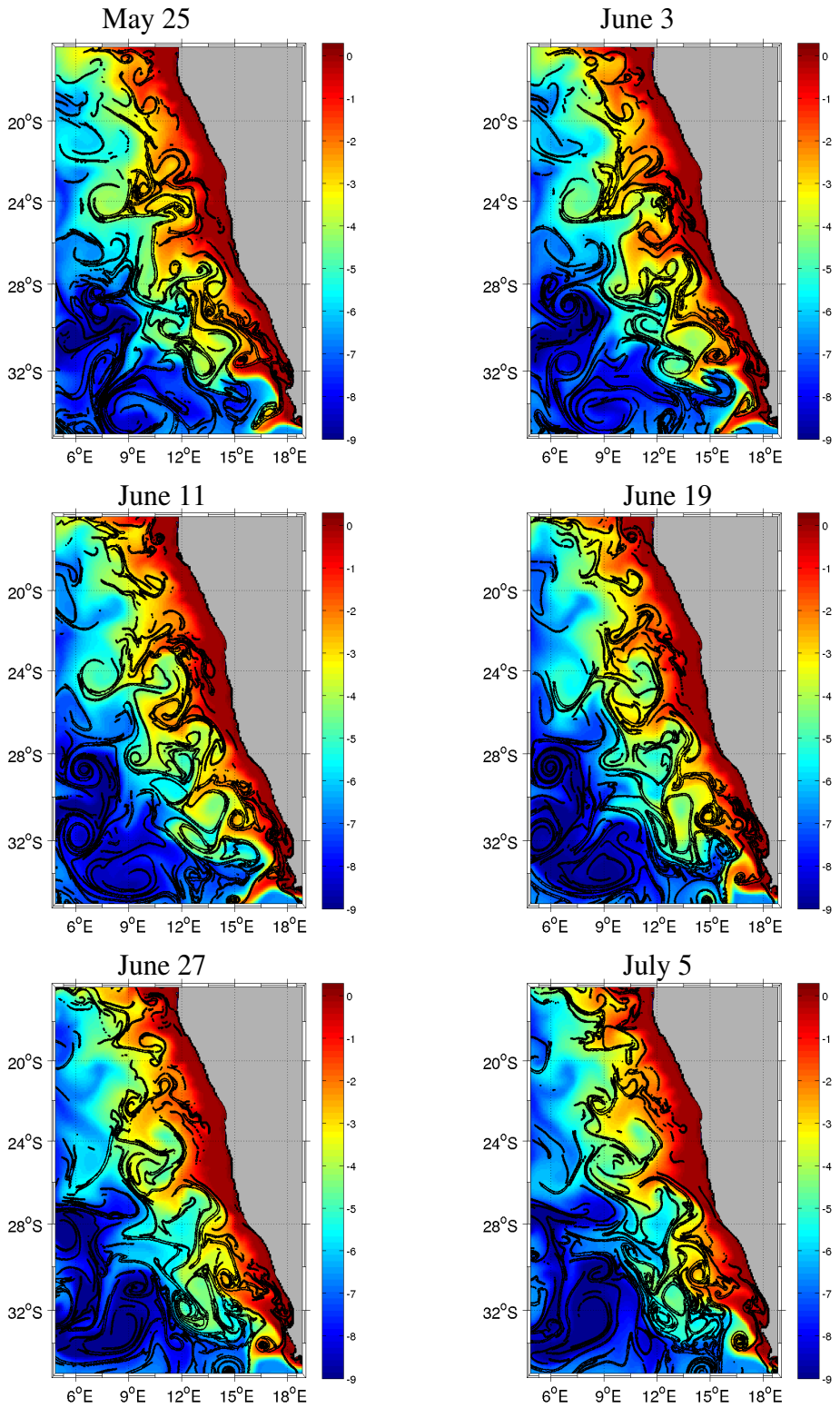

Figure 6: Snapshots every 8 days of large (top 30%) values of FSLE superimposed on P concentrations calculated from *ROMS1/12* in mg/m^3. Logarithmic scale for phytoplankton concentrations is used to improve the visualization of the structures

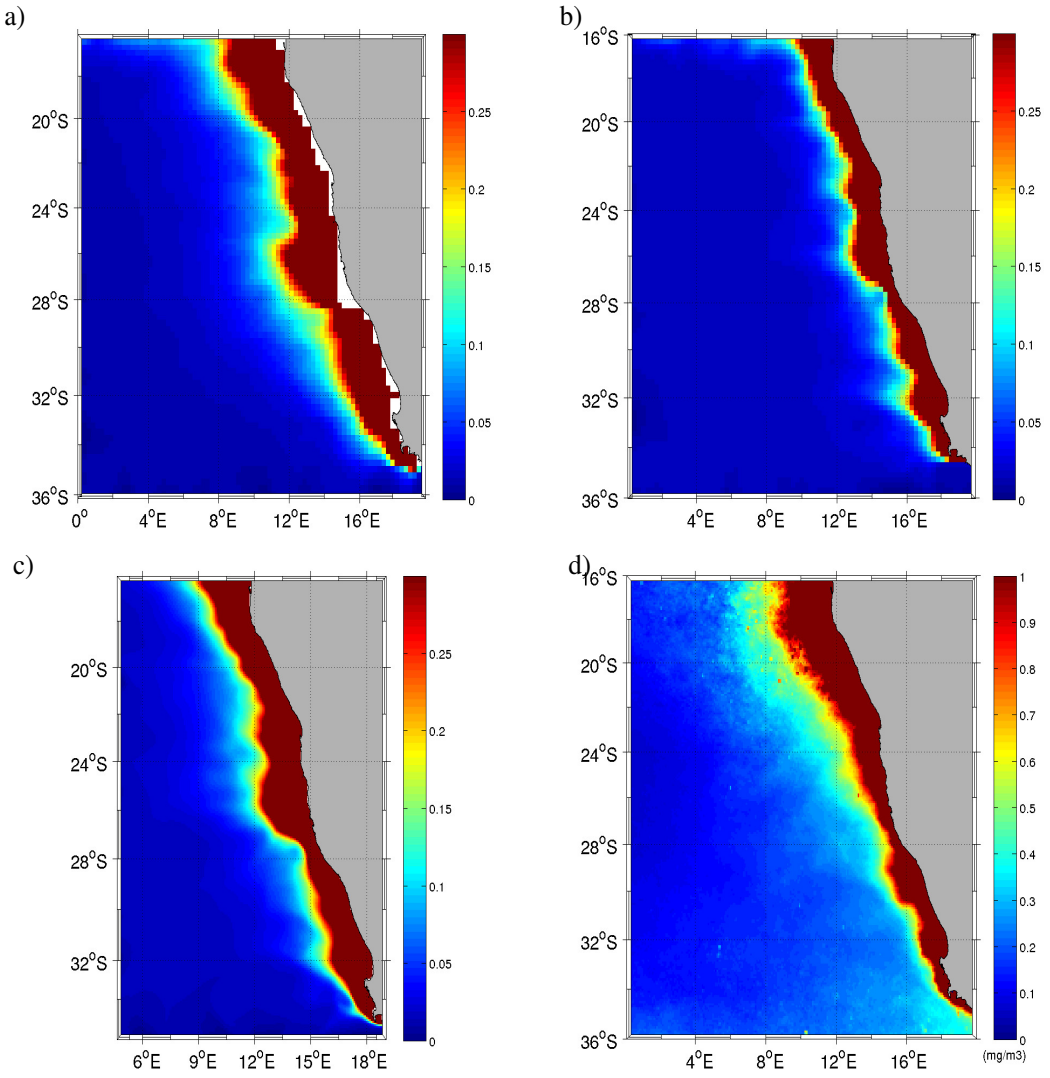

Figure 7: Spatial distribution of the time average of phytoplankton concentrations: a) Three years average using *Satellite1/4*, b) One year average from *ROMS1/4*, c) One year average from *ROMS1/12*, d) Three years average of monthly SeaWIFS data. The units of the colorbar are mg/m^3.

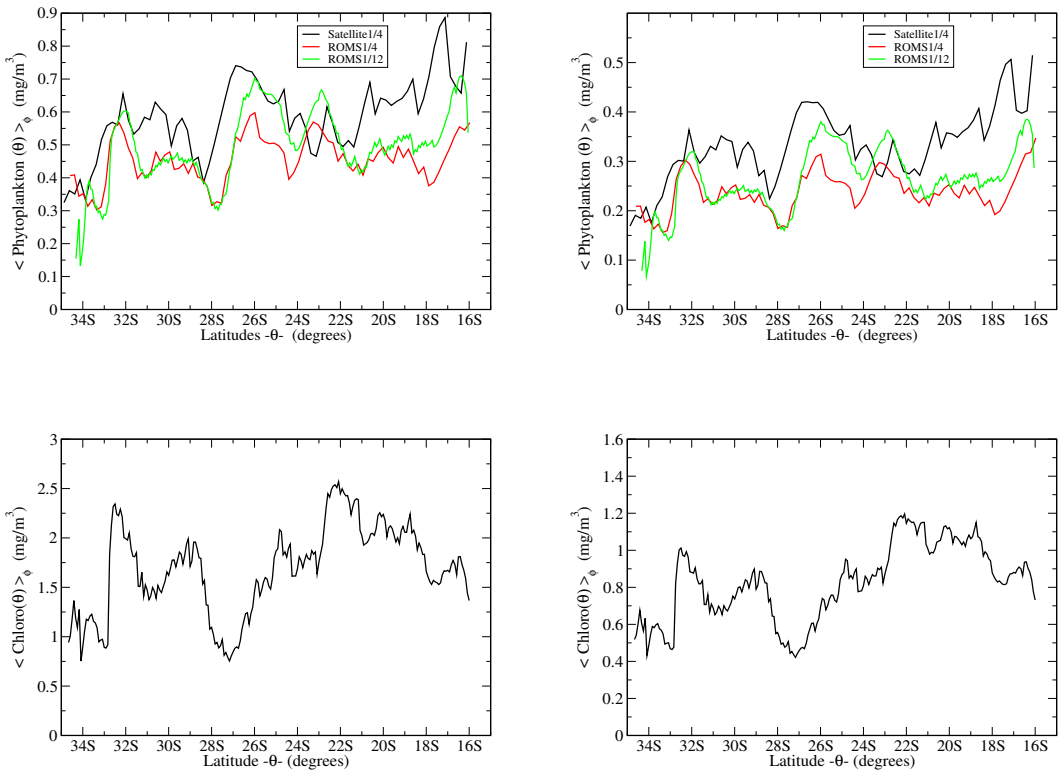

Figure 8: Zonal mean, over a 3 degrees (left) and 6 degrees (right) width coastal band, of the time averages of modelled phytoplankton (upper plots) and derived from satellite (lower plots) plotted as a function of latitude.

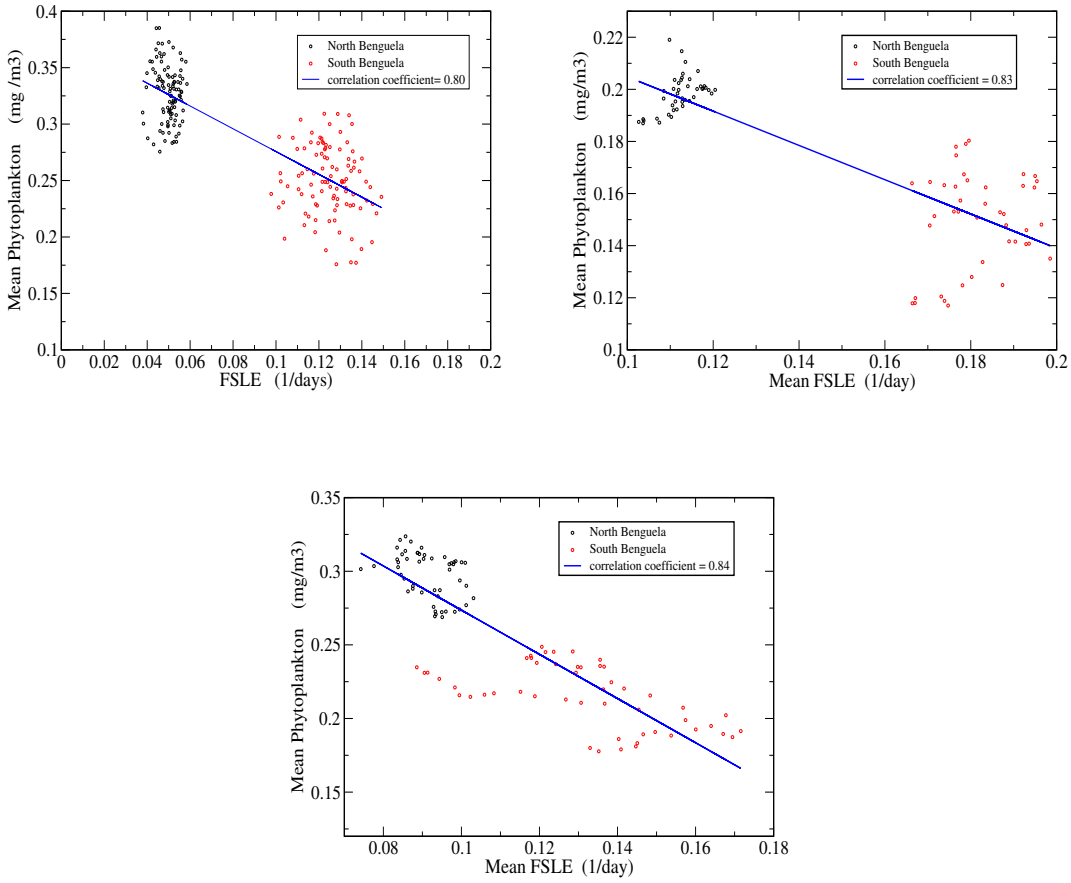

Figure 9: Weekly values of spatial averages of phytoplankton versus weekly values of spatial averages of FSLE, where the average are over the North and South subareas of Benguela. a) *Satellite1/4*, b) *ROMS1/4* and c) *ROMS1/12*

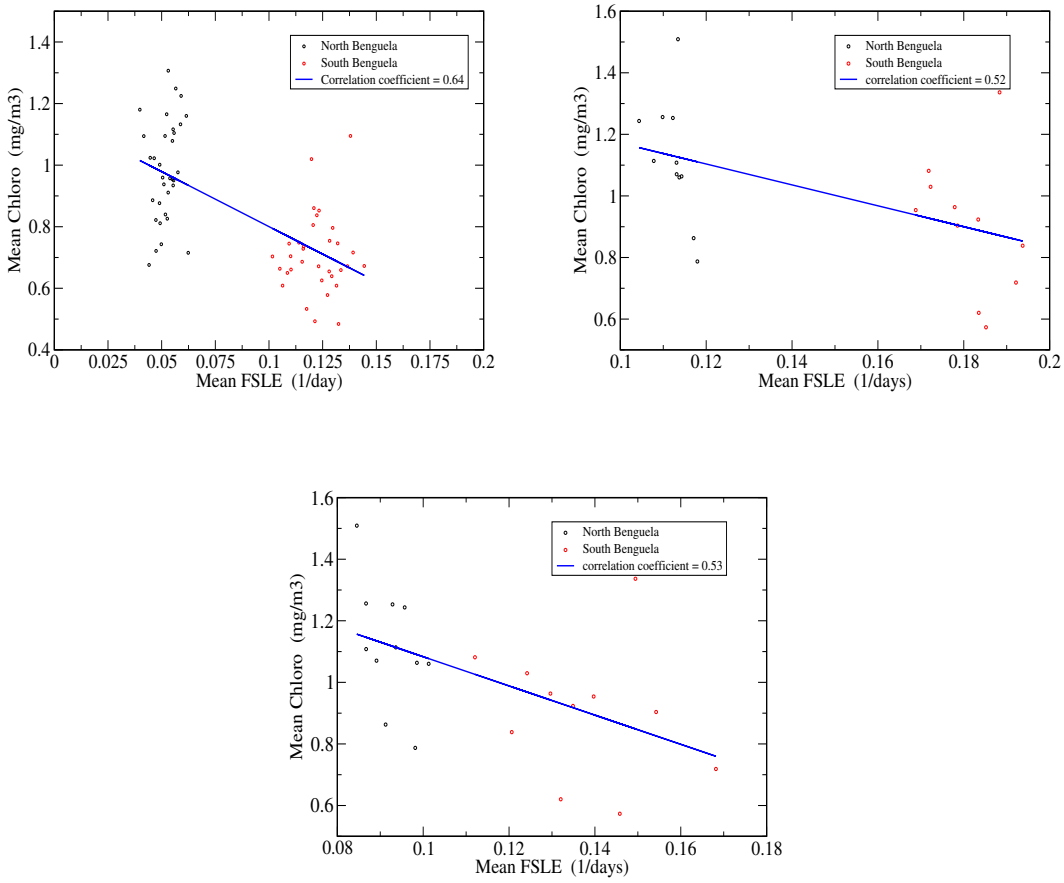

Figure 10: Monthly values of spatial averages of Chlorophyll from SeaWIFS data versus spatial average of FSLE, where the average are over the North and South subareas of Benguela. FSLE values are from a) *Satellite1/4*, b) *ROMS1/4* and c) *ROMS1/12*.

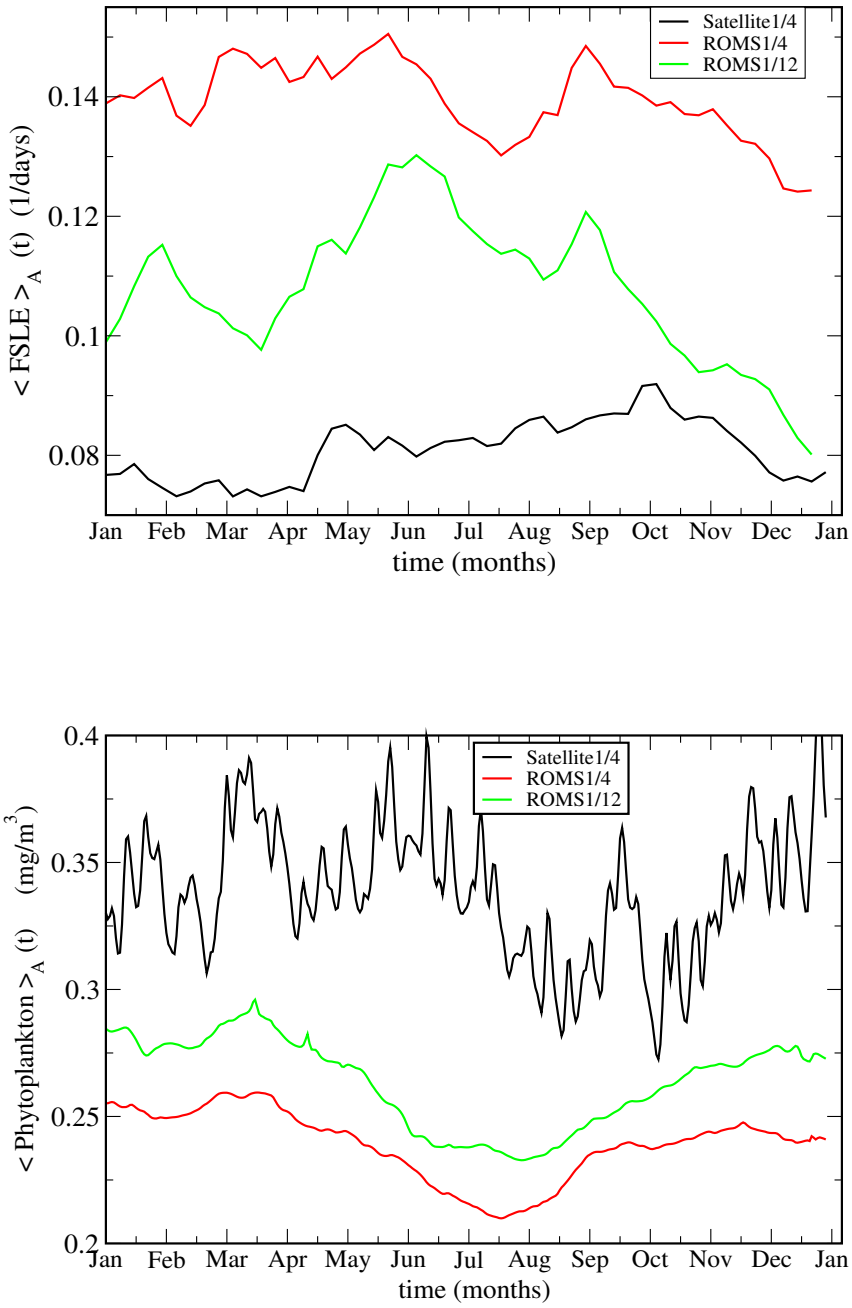

Figure 11: Temporal evolution of horizontal mixing (Spatial average of FSLEs) for the three velocity data sets (top). Temporal evolution of spatial averages of simulated phytoplankton for the three velocity data sets (bottom).

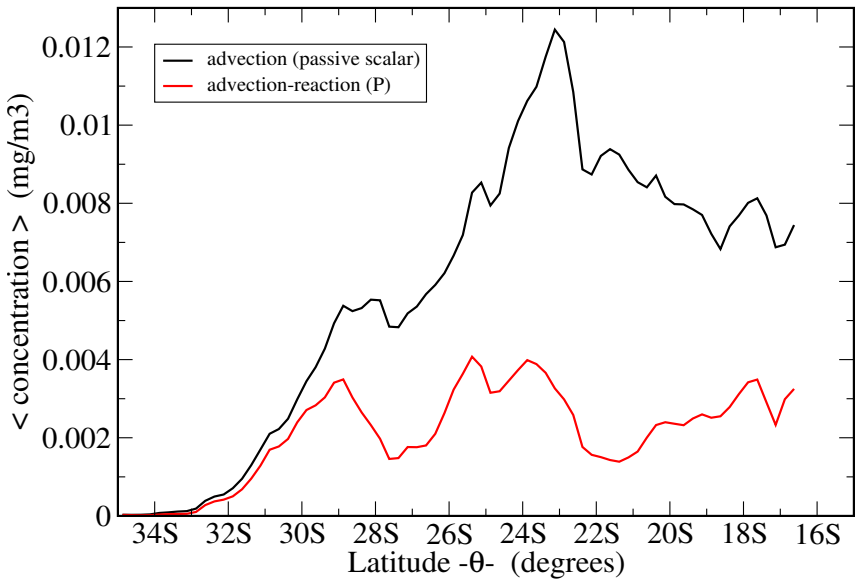

Figure 12: Normalised comparison of the time averages of a passive scalar (advection only) and of P (advection-reaction), as a function of latitude.

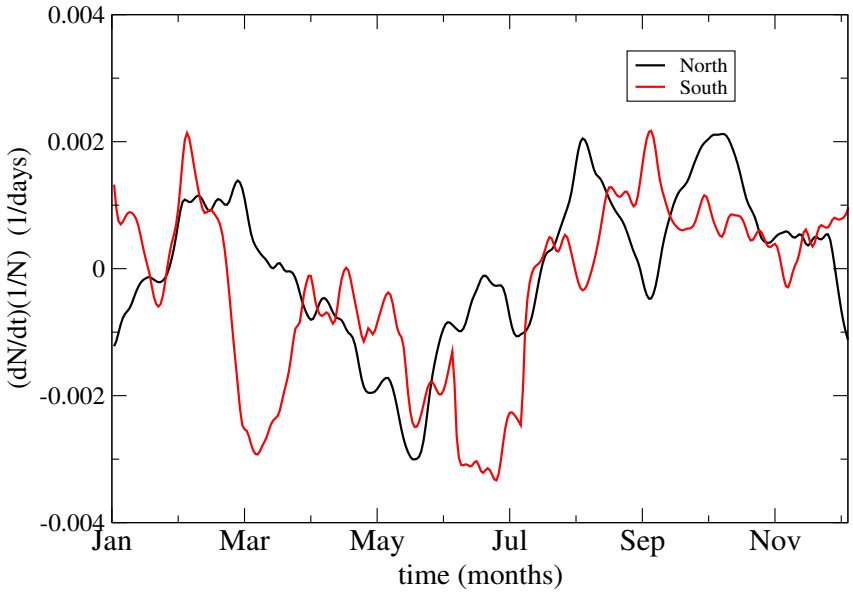

Figure 13: Time evolution of the spatial average of the per capita growth rate of nutrients for the *ROMS1/12* case.